Numerical Methods in Civil Engineering, 6-2 (2021) 66-76

Numerical Methods in Civil Engineering

Journal Homepage: https://nmce.kntu.ac.ir/

Optimization of through-bolt steel beam connection to CFST column reinforced with rib plates using RSM method and MCEO algorithm

Khadijeh Ghanbari Soumeh* and Hoseein Parvini Sani**

ARTICLE INFO

RESEARCH PAPER

Article history:
Received:
June 2021.
Revised:
August 2021.
Accepted:
August 2021.

Keywords:
CFST connection,
Optimization problem,
MCEO algorithm,
Response surface method,
Rib plates

Abstract:

Today, one of the most important engineering requirements is to ensure optimal design with best possible seismic performance of structures. To this end, the present paper aims to apply the optimization process for the design of the through-bolt steel beam connection to the concrete-filled steel tube (CFST) column reinforced with rib plates. This study employs a multi-level cross-entropy optimizer (MCEO) algorithm along with response surface method (RSM) and finite element method (FEM) to establish the objective functions and constraints. The variables considered are the rib plate geometry and the steel and concrete strength parameters. In order to overcome problems, optimization is performed to increase the load-bearing capacity of the connection and to satisfy the constraints. Adopting this smart solution eliminates the need to connect finite elements for loop optimization and provides an explicit function for system performance. The results show that a very accurate analytical model can be developed to describe system performance using this process. This solution can optimize the performance of several systems that require a large amount of analysis and solve a wide range of structural optimization problems.

1. Introduction

The safety of the occupants is of great importance in the design of structures, considering the seismic forces that result in financial losses and undesirably affect the performance of the structures [1, 2, 3]. On the other hand, both safety and economy should be considered in the design of the structures. Structural safety is always the main concern that an engineer should take into account, while economic design should also be considered by relying on the optimization problem [4]. Several design variables can be considered in the formulation of the optimization problem [5, 6]. The structural optimization problems can be divided into three open research areas: (1) optimization, (2) modeling and solving new structural engineering problems as optimization problems, and (3) analysis [7]. A deterministic optimization problem is often expressed as a set of equations:

$$\begin{aligned} &\text{Minimize/Maximize} \quad f(\boldsymbol{x}) \\ &\textit{Subject to} \quad g_i(\boldsymbol{x}) \le 0 \quad i = 1, \dots, m \\ &\textit{and/or} \quad h_j(\boldsymbol{x}) = 0 \quad j = 1, \dots, l \\ &\textit{in which} \quad L_b \le \boldsymbol{x} \le H_b \end{aligned} \tag{1}$$

where f is the objective function of the problem, which concerns the minimization or maximization of a particular problem; $\boldsymbol{x}$ is a vector with n elements that expresses the deterministic variables of the desired n-dimensional problem; and g_is and h_js represent equality and inequality constraints of the problem, respectively. m and l also show the number of these constraints. A design that satisfies all the constraints is called a "feasible" design. A design that violates even one of the constraints is called an "infeasible" design. Here, L_b and H_b show the lower and upper bounds of the variables, respectively [8, 9]. One of the most important issues in the connection between science and practice is the proper use of optimization methods in construction projects. Hence, in the implementation of many current projects, there is either non-optimal overdesign, which leads to increased costs, or underestimated design, which leads to structural failure [10]. Therefore, it is important to properly apply the existing optimization methods and integrate them into problem-solving.

* *M.Sc, Department of Civil Engineering, Zanjan Branch, Islamic Azad University, Zanjan, Iran*
** *Corresponding author: Assistant Professor, Department of Civil Engineering, Zanjan Branch, Islamic Azad University, Zanjan, Iran, Corresponding author, E-mail: hossein.parvini_sani@iauz.ac.ir*

In recent decades, extensive research has been conducted on the behavior of moment connections in concrete filled steel tubes (CFSTs) under cyclic loading, leading to new connections and the development of regulations for them [11, 12]. In addition to conducting extensive research on moment connections in CFST columns, it is essential to conduct further studies on CFST connections and their complete frames [13]. However, limited laboratory equipment and economic reasons prevent many experiments from being carried out on a practical scale. The finite element method (FEM) can also be used to fully simulate the effects of imposed loads, such as hysteresis or seismic loads [14, 15].

The use of thorough-bolting method for connecting beams to CFST columns is one of the accepted connections. The existing studies show that the bolted connection of steel beams to CFST columns has good earthquake-resistant performance [16]. Woa et al. [17] conducted a study on the seismic behavior of CFT columns and H-beams with two-sided bolted connections. The results showed that the resistance to seismic conditions exceeds the seismic design criteria in the United States and Taiwan. Therefore, two-sided bolt connections have excellent earthquake resistance and, as expected, very good performance in this structural system. Wang et al. [18] conducted a study on the columns of the concrete-filled steel tubes to evaluate the behavior of platform connections. According to the obtained results, in the structures with moment-resisting composite frames, closed two-bolt connections are reliable and efficient. Wang et al. [19] performed experimental and numerical analyses on the connections of a single-sided bolt-nut moment to CFTST columns. They also investigated the mechanical behavior of the platform connecting the bolts and nuts of the CFTST columns through experimental and numerical analyses. These creatively closed double bolts and nuts are proposed in mid-rise and low-rise buildings with reliable and effective solutions.

There has been a lot of research in the field of connection optimization, the most important of which are mentioned. Zhang et al. [20] performed seismic optimization analysis of vertical stiffener connection to CFST column in a meta-model-based study. In this study 14 models in two series were designed and numerically analyzed based on the results of quasi-static tests of vertical stiffener connections to L-CFST columns. Yang et al. [21] researched the optimization of concrete casting in steel tubular ribs for long-span CFST arch bridge. Nguyen et al. [22] evaluated the possibility of using a feedforward neural network (FNN) to predict the axial capacity (Pu). Furthermore, an evolutionary optimization algorithm, namely invasive weed optimization (IWO), was used for tuning and optimizing the FNN weights and biases to construct a hybrid FNN–IWO model and improve its prediction performance. Hanoon et al. [23] proposed new numerical models for modeling the flexural capacities (Mu, Ki, and Ks of CFST beams under static bending load. For this purpose, numerous existing experimental and numerical results of CFST beams were collected for developing a new numerical model called hybridized artificial neural network (ANN) model with particle swarm optimization (PSO) algorithm. Pachideh et al. in 2020 [24] studied the impact of temperature rise on the performance of Concrete-Filled Double Skin Tubular Steel Columns with prismatic geometry. they also investigated the seismic performance of the concrete-filled double skin steel tubular columns whose geometry is prismatic in 2021 [25].

The present study investigates the effect of using rib plates when connecting steel beams to CFST columns with through bolts, considering the geometric variables, namely rib plates and material strength. The main purpose of measuring the variables is to obtain the degree to which the geometric and strength parameters of the rib plate affect the load-bearing capacity and stress of the models. This problem was solved using a metaheuristic multi-level cross-entropy optimizer (MCEO) algorithm integrated with response surface method (RSM) and FEM. This strategy has not been carried out in any previous work with these variables. It is hoped that by applying this solution and sensitivity analysis of the parameters, a clearer view of the performance of the CFST connections will be obtained. Various optimization problems in the fields of mechanics, civil engineering, electricity, etc. (in which another parallel solver is needed) can be also simplified and solved by using this technique.

2. Optimization method

2.1. Multi-level cross-entropy optimizer (MCEO) algorithm

The MCEO algorithm uses multiple averages in each iteration simultaneously and in parallel to guide the samples. Incorporating the basic concepts of cross-entropy, this method continues until a suitable level of stability is reached [26].

2.1.1. Initial implementation

The mean driving point in this algorithm is called the 'average' in the search process. According to the equation, the averages are evenly distributed across the search area to create the initial conditions of the algorithm (2).

$$Averages = {}_1^n[P\ (H_b - L_b)] \quad (2)$$

In this equation, $Averages$ shows the matrix of medium-sized particles, which are distributed evenly in the n-dimensional space of the problem in the first iteration. P is a random number between 0 and 1. The lower and upper limits of the research area are denoted by L_b and H_b, respectively. In MCEO, several search particles known as 'search agents' are distributed around the mean. Therefore, in the first iteration of the algorithm with a value of the first standard deviation with normal distribution, the search agents are distributed around the averages. In the first search agent iteration, the MCEO attempts to cover as much search space as possible. Therefore, the first suggestion in the MCEO [26] is the initial standard deviation of the search particles with Equation (3):

$$\sigma_{Initial} = 2 \times \frac{(H_b - L_b)}{n_{Averages}} \quad (3)$$

where $n_{Averages}$ and $\sigma_{Initial}$ represent the number of media in the first iteration and the standard deviation of the algorithm, respectively. These steps are illustrated in Figure 1.

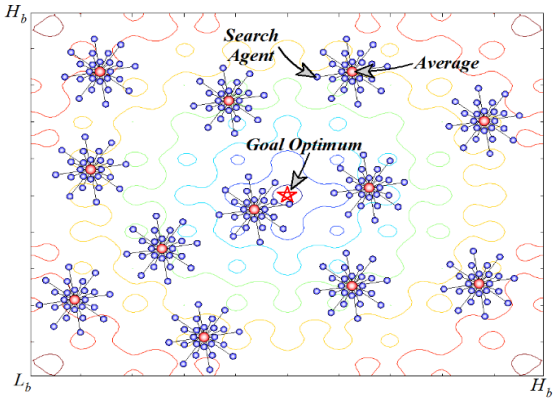

Fig. 1: Initial implementation of MCEO [26]

2.1.2. Search parameters in MCEO

The motion applied to the search particles during each iteration cycle should endow the samples with five different functions, as shown in Figure 2. The following processes were implemented to include these five steps in the MCEO: The first step is to generate a complete matrix of search particles and solutions. This matrix is sorted by the obtained solutions so that the first row of the complete matrix contains the best position with the best solution. The new averages of the next iteration are then $n_{Averages}$ of the particles from the top of this matrix (including the best positions and their corresponding solutions, except the first solution). To store the best solution, it is important to select the first row of the comprehensive matrix in the following iteration of the search particle. The best position is also lost in the next iteration when the new average is selected. For instance, if the number 1 is taken as the average of 10 random numbers and the distribution itself is formed around it with a standard deviation, this number itself may not exist accurately. The motions of the search particles are therefore performed according to the cases that have a tendency to the global optimum and have the best condition. In this way, property (a) (attraction) is satisfied by these five cases [20].

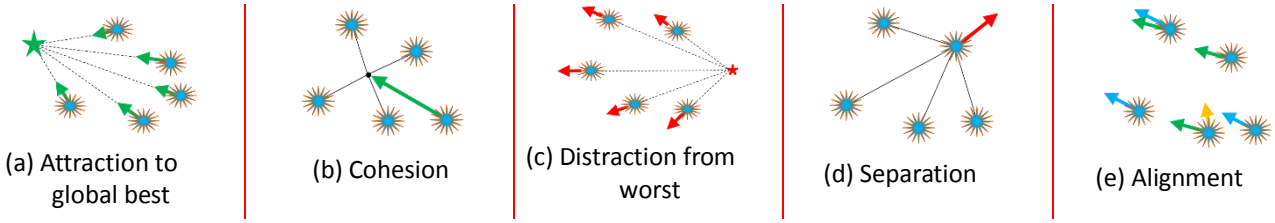

Fig. 2: Basic properties of particle motion in metaheuristic optimization algorithms [19]

2.1.3. Computational parameters of MCEO

The cost of meta-heuristic algorithms is calculated according to the number of average searches and the number The search particles appear in blue in Figure 3a and their corresponding solutions are denoted in red. Here, It is a replication counter algorithm in which best solutions are selected as the averages of the following iteration after sorting out the particle position according to its solutions in the It^{th} iteration. The percentage is created randomly, as shown in Figure 3b. A linearly decreasing coefficient called the "standard reduction coefficient" (SRF) is introduced to change the standard deviation of each average. The standard deviation of averages decreases with appropriate relative positions. The standard difference between averages increases with relatively inappropriate positions. Therefore, step (e) (alignment) in Figure 2 is already included in the MCEO. Figure 4 presents the effect on particulate matter distribution by applying the SRF coefficient [26].

of particles, length of search area, number of problem areas, and maximum iterations. Taking the previously mentioned extensive matrix sorting mechanism into consideration, an appropriate solution is provided to improve the problem-solving speed and prevent the trapping of the local optima of the new algorithm. One of the most important achievement of this strategy is high-accuracy and low-speed search where the optimum point probability is high and low-accuracy and high-speed search where the optimum point probability is low [20].

Therefore, the solutions provided by the standard deviation of the search particle are used to meet steps b (cohesion) and c (distraction) of the items in Figure 2. In situations with either improper solutions or the best solutions, the standard deviation in each step should increase (the better the solution, the lower the standard deviation). This process is expressed by $\left(\frac{i}{n_{Averages}}\right)$, where i is the row number to select the media out of the extensive matrix. The third power of the above relation is suggested in this algorithm, which reduces or increases the standard deviation and parallelization of the CEs to find a stable solution to a wider range of problems. Parameter φ is also included to consider and apply the impact to the standard deviation of the search particles of the problem dimension. According to the explanations given, Equation (4) is proposed for the standard deviation of search particles for different purposes [26]:

$$\sigma_i = \left(\frac{i}{n_{Averages}}\right)^3 \left(\frac{H_b - L_b}{\varphi}\right) \quad , \quad \varphi = \frac{nVar^2}{n_{Averages}} \tag{4}$$

where σ_i expresses the standard deviation of the ith mean and $nVar$ denotes the number of dimensions of the problem. It is also suggested in the present MCEO step for finding new and unknown situations that 20% of the worst averages are ignored and substituted by new random averages in this algorithm. Thus, property (d) (separation) is also included in the algorithm among the items shown in Figure 2. The above-mentioned items are illustrated in Figure 3.

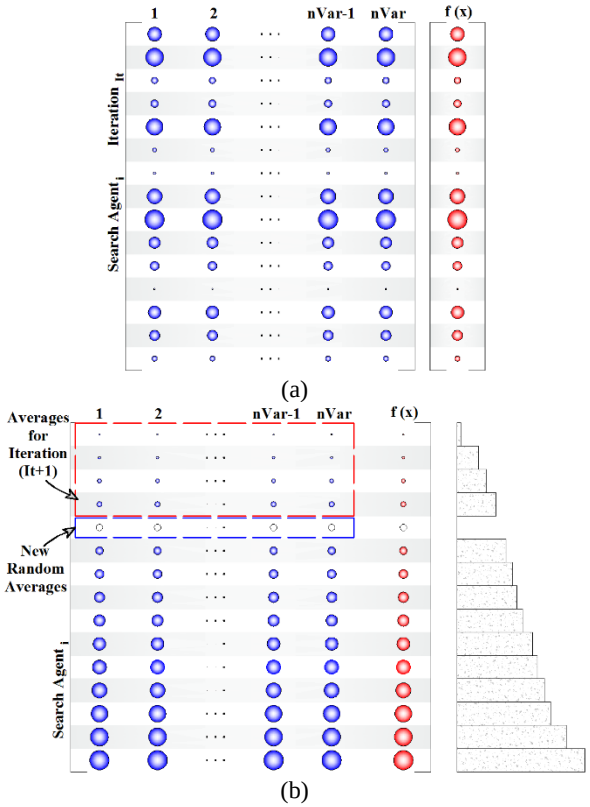

Fig. 3: a) Solution of different particles, b) sorting based on solutions and forming a comprehensive matrix [26]

Updating the standard deviation leads to a clear and coherent pattern that distributes the search particles over the available space. After a few iterations of the pattern, the best averages are slightly different and the exploitability is very high. Besides, the search particles formed around unsuitable averages with high standard deviation are an efficient way of space exploration. Figure 5 clearly shows this process [26]. Another way to avoid trapping in local optima in MCEO is to stochastically generate a percentage of the averages. The particles outside the potential space are symmetrical about the boundary of the problem space due to the high standard deviation of certain media.

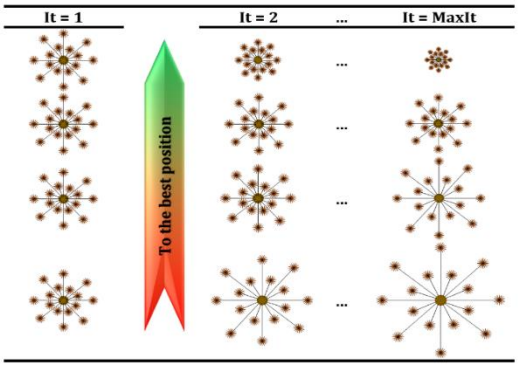

Fig. 4: Effects of SRF on decrease and increase in standard deviation of search particle distribution around averages [26]

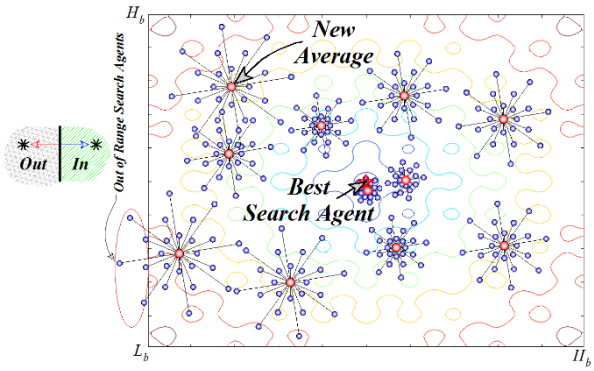

Fig. 5: Motion of particles in MCEO in near (suitable) and far (unsuitable) positions compared to optimal position [26]

2.2. Response Surface Method (RSM)

In RSM, a lower bound and an upper bound are first defined for the variables. The distance between the bounds is then divided into equal values according to the accuracy required to represent the functions. Design of experiments (DOE) is an important aspect of RSM. Originally developed to fit experimental models, this strategy can also be used in numerical experiments. The DOE aims to select the points to evaluate the response. The choice of experimental designs can greatly affect the accuracy of the estimation and the cost of building the surface response model. After selecting the experimental design, the model equation is determined and its coefficients are predicted. The RSM model is normally the equation or reduction in the form of the whole quadratic model with respect to the quadratic model [27]:

$$Y = X\zeta + \varepsilon \tag{5}$$

$$\begin{bmatrix} y_1 \\ y_2 \\ . \\ . \\ . \\ y_n \end{bmatrix}_{n\times 1} = \begin{bmatrix} 1 & x_{11} & x_{12} & . & . & . & x_{1k} \\ 1 & x_{21} & x_{22} & . & . & . & x_{2k} \\ \dots & \dots & \dots & \dots & \dots & \dots & \dots \\ \dots & \dots & \dots & \dots & \dots & \dots & \dots \\ \dots & \dots & \dots & \dots & \dots & \dots & \dots \\ 1 & x_{n1} & x_{n2} & . & . & . & x_{nk} \end{bmatrix}_{n\times k} \begin{bmatrix} \zeta_0 \\ \zeta_1 \\ . \\ . \\ . \\ \zeta_k \end{bmatrix}_{k\times 1} + \begin{bmatrix} \varepsilon_1 \\ \varepsilon_2 \\ . \\ . \\ . \\ \varepsilon_n \end{bmatrix}_{n\times 1} \tag{6}$$

where ζ_{k0}, ζ_{ki}, ζ_{kii}, and ζ_{kij} are constant, linear, quadratic, and regression interaction coefficients, respectively. Besides, x_i and x_j are the independent coded variables. Equations (5) and (6) provide the matrix notation of this process. The above system is solved by the least square method (LSM), and the coefficients of the equation are then obtained. Afterward, the solution is predicted to solve the above equation. Compliance with the model should then be verified with experimental data. Various methods, such as residual analysis, root mean square error, and malfunction test can be employed for this purpose [22, 23].

3. Finite element model validation

In recent years, FEM has been recognized as a powerful tool for structural analysis [30]. Therefore, in this study, the connection of the beam to the CFST column developed by Abaqus software was selected as a validation example from the study of Wu LY et al. [31]. The support and loading conditions and the geometric properties of the sample connection in the laboratory are illustrated in Figure 6.

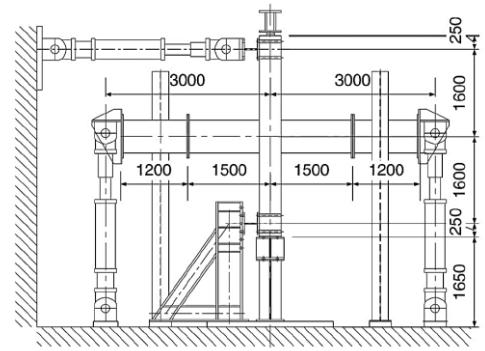

(a)

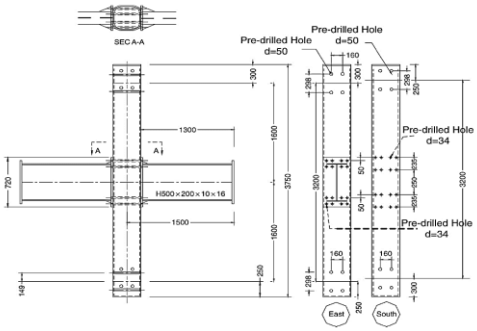

(b)

Fig. 6: (a) Schematic view of boundary conditions and loading, (b) geometric characteristics of test connection [29]

Tables 1 shows the dimensions and material specifications of all parts used in this study [31].

One of the connection samples (i.e., FSB-8) was modeled in Abaqus software for validation under the conditions of the reference article. In this modeling, solid eight-node elements are used to model all beam elements, steel tubes, triangular stiffener, end plate, bolts, and concrete core. The concrete damaged plasticity criteria for concrete, and plastic failure for steel materials (including the von Mises yielding and hardening criteria) were used to define the mechanical properties of materials in the nonlinear region. In this study, the connection between the connected edges of all elements is modeled using the loading sample with the tie limit. The reason is the lack of study on the welding behavior at micro models and the assumption of the optimal welding conditions (complete continuity and no weld failure during loading). The hard contact constraint was used to represent the behavior of the contacting surfaces between: the bolts and the concrete, the surface of nuts and the end plate, the end plate with the column and the steel column with cement core). The concrete plasticity failure profile was also used to define the concrete behavior. The dynamic analysis was used for this example. The loading protocol is presented in Figure 7, which was used for the loading. The fixed support was defined for both ends of the column. Figure 8 depicts the final constructed model and the stress contours in the numerical sample.)

Table. 1: Dimensions and material specifications of all parts [31]

Specimen	Column section (A572 Grade 50) (mm)	t (mm)	B/t	Filled of concrete	Beam section (A36) (mm)
FSB-6	□400 × 400 × 6 × 6	6	66	YES	H500 × 200 × 10 × 16
FSB-8	□400 × 400 × 8 × 8	8	50	YES	H500 × 200 × 10 × 16
FSB-10	□400 × 400 × 10 × 10	10	40	YES	H500 × 200 × 10 × 16

Specimen	Steel												Concrete
	Beam (rolled shape)												
	Web				Flange				Column (built up)				
	σ_y (MPa)	σ_u (MPa)	ε_y (%)	ε_u (%)	σ_y (MPa)	σ_u (MPa)	ε_y (%)	ε_u (%)	σ_y (MPa)	σ_u (MPa)	ε_y (%)	ε_u (%)	$\bar{f}'_c$ (MPa)
FSB-6	337.5	427.0	0.19	28.00	303.4	425.8	0.15	36.50	431.0	521.3	0.21	28.75	25.26
FSB-8	337.5	427.0	0.19	28.00	303.4	425.8	0.15	36.50	381.8	501.6	0.17	28.80	29.29
FSB-10	337.5	427.0	0.19	28.00	303.4	425.8	0.15	36.50	356.5	474.7	0.19	35.30	27.185

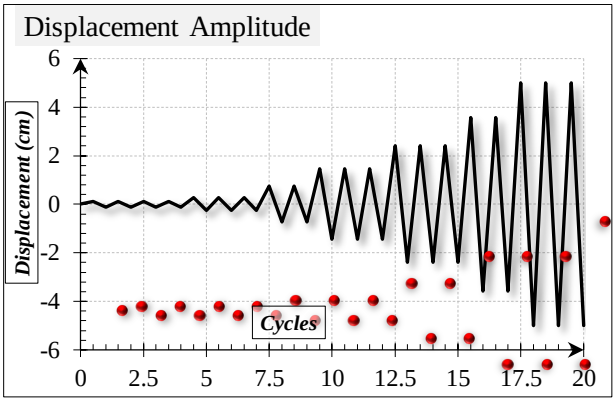

Fig. 7: The loading protocol [31]

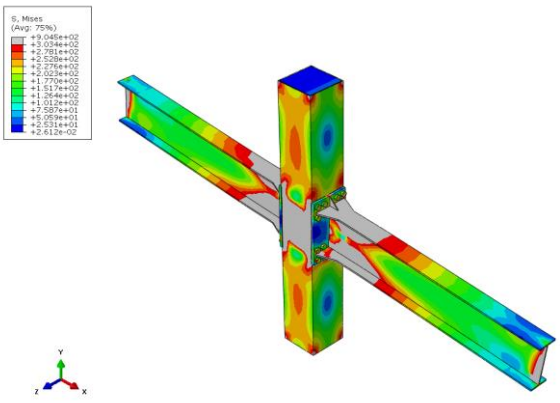

Fig. 8: Final meshed model & overall stresses induced in numerical sample

The data recorded in the numerical analysis software were compared with the experimental diagram in Figure 9. The shear capacity of the connection was found to be 315,657 kN, while it was found to be 302,362 kN in the Abaqus simulation with an error of about 4%. As can be seen, the results are quite close to the experimental results. Due to the very complex nature of plastic and nonlinear concrete, a small error is observed in the output.

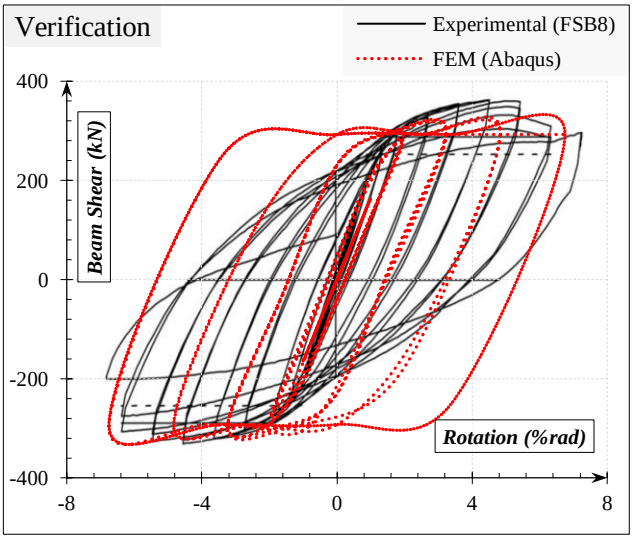

Fig. 9: Diagram of comparing experimental sample with numerical sample

4. Optimization problem of CFST connection

4.1. Design variables

For explicit relationships in the representation of system performance, the RSM developed in Design-Expert software was used. The models are developed based on the validated model. Five parameters are considered as variables in this regard. The first three variables are related to the geometry of the connected rib plates, which can be seen in Figure 10, and the last two variables are steel yield strength and concrete strength. The thickness of the connected upper and lower rib plates varies between 6 and 14 mm. As illustrated in Figure 11a, the levels of -1 and +1 for this variable are 8 and 12 mm, respectively, by mapping the right intervals -2 to +2. The lengths of the upper and lower rib plates, for which the levels of -1 and +1 are equal to 80 and 120 mm in the range of 60 and 140 mm, respectively, are similar in Figure 11b. According to Figure 11b, the lateral rib length in the range of 120-280 mm, the steel yield strength in the range of 260-420 MPa, and the concrete strength in the range of 20-40 MPa are also mapped to 1- and 1+ alpha levels equal to 2 in the response surface, as shown in Figure 12.

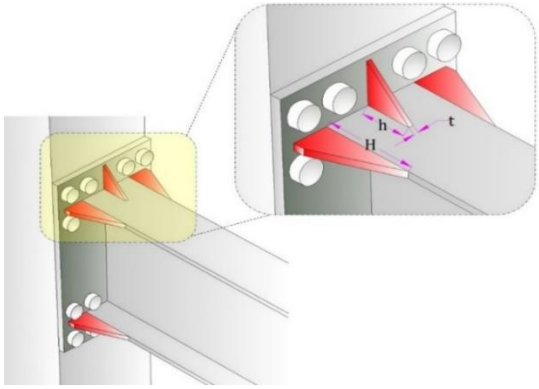

Fig. 10: Geometric variables of the connecting rib plates

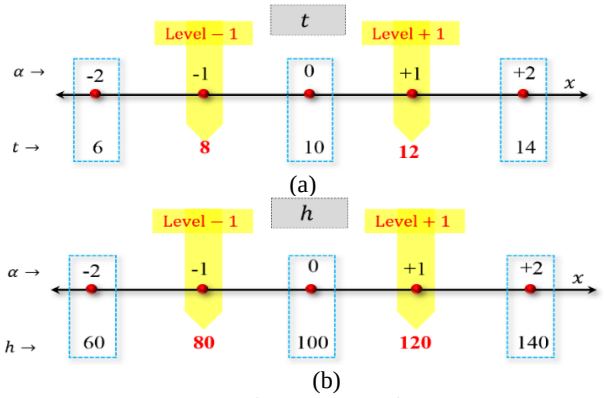

Fig. 11: (a) Alpha levels for thickness of upper and lower rib plates, (b) alpha levels for length of upper and lower rib plates

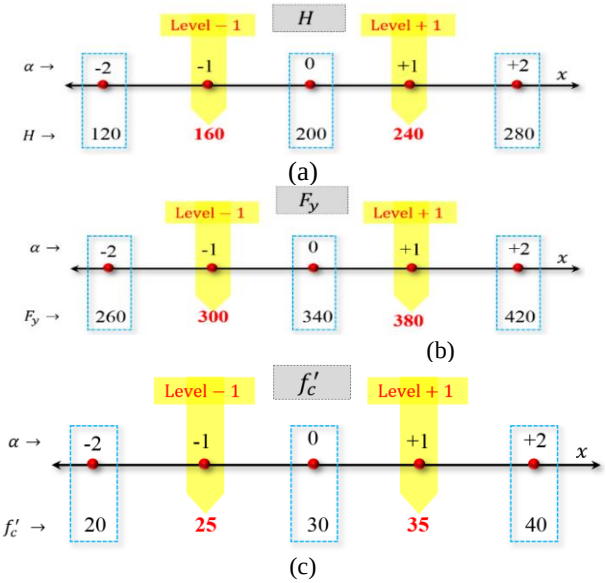

Fig. 12: (a) Alpha levels for length of connected lateral rib plates, (b) alpha levels for steel yield strength, (c) alpha levels for concrete strength

To examine all the above possible scenarios with five parameter in each of five cases, it is necessary to develop $5^5 = 3125$ models in the Abaqus software. At this point, however, the design expert software reduced the required models to 50. In any case, the simulation should be performed using ABAQUS to extract the output including the shear capacity and the maximum stress at the connection. This issue is explained in the following section.

4.2. Response surface results and creation of analytical functions

Based on the RSM principles used in the Design-Expert software, the introduced models are presented in Table 2. This table contains 50 models in which the individual values of the five variables are given. These 50 models should be designed based on the validated model, and the Abaqus software should estimate the stress and load-bearing capacity of each model. As can be seen, the model numbers appear in the first column of this table. The second through sixth columns provide the values of the variables, including rib plate thickness (mm), rib plate length (mm), lateral rib plate length (mm), steel yield strength (MPa), and concrete strength (MPa). The 7th and 8th columns of this table show the shear capacity (kN) and maximum stress (MPa) obtained by the Abaqus model.

Table 2: Models developed by response surface

Model	t (mm)	h (mm)	H (mm)	F_y (MPa)	f'_c (MPa)	R (kN)	S (MPa)
Model1	8	80	240	380	35	314.52	222.75
Model2	10	100	200	340	30	283.84	234.79
Model3	12	80	160	300	35	270.18	260.17
Model4	10	100	200	420	30	335.23	189.19
Model5	10	140	200	340	30	329.78	194.47
Model6	8	120	160	300	35	273.03	262.99
Model7	8	120	160	300	25	222.37	340.06
Model8	12	120	160	380	35	359.5	177.74
Model9	10	100	200	260	30	241.94	287.97
Model10	8	80	160	300	35	217.33	350.91
Model11	8	80	160	300	25	164.79	419.86
Model12	10	100	200	340	30	281.91	243.11
Model13	10	100	200	340	30	286.15	243.80
Model14	12	80	160	300	25	211.10	344.17
Model15	8	80	240	300	35	270.91	248.63
Model16	8	120	240	300	25	256.33	253.09
Model17	10	60	200	340	30	234.03	286.98
Model18	12	80	240	300	35	301.53	216.41
Model19	6	100	200	340	30	234.06	280.87
Model20	8	120	160	380	35	308.79	217.34
Model21	8	80	240	300	25	212.51	319.95
Model22	12	120	160	300	35	322.17	215.83
Model23	8	120	160	380	25	261.62	259.44
Model24	12	80	240	380	35	347.72	185.00
Model25	8	120	240	380	35	371.06	183.79
Model26	12	80	160	380	35	323.72	221.42
Model27	10	100	200	340	30	285.35	243.25
Model28	12	80	240	300	25	254.46	255.06
Model29	12	120	240	380	25	350.09	183.48
Model30	12	80	160	380	25	261.13	251.34
Model31	10	100	120	340	30	241.39	277.61
Model32	12	120	160	300	25	257.85	266.26
Model33	12	120	240	300	25	313.38	212.40
Model34	8	80	240	380	25	267.92	259.05
Model35	12	120	240	380	35	218.08	293.75
Model36	12	120	160	380	25	300.06	214.85
Model37	10	100	200	340	30	281.80	236.53
Model38	14	100	200	340	30	328.82	202.06
Model39	10	100	200	340	30	284.98	241.15
Model40	10	100	200	340	20	239.65	294.40
Model41	10	100	200	340	30	276.54	225.84
Model42	8	80	160	380	35	257.85	252.49
Model43	8	80	160	380	25	221.06	347.35
Model44	12	120	240	300	35	342.67	170.80
Model45	8	120	240	380	25	322.32	212.17
Model46	12	80	240	380	25	316.88	204.97
Model47	10	100	200	340	30	286.59	245.41
Model48	10	100	280	340	30	336.60	199.05
Model49	10	100	200	340	40	326.38	194.70
Model50	8	120	240	300	35	309.43	211.75

Equations (8) and (9) are provided based on the response surfaces methodology by using the design expert software. The values in Table 2 (columns 2 to 5) were given to the software as input variables, and the column 6 and 7 were introduced as outputs, to obtain these equations. Software analysis was also adjusted to create a quadratic equation, and the interaction of the input parameters was also considered.

$$R(t,h,H,F_y,f'_c) = -444.22183 + 23.43675 * t + 2.02854 * h + 0.35536 * H + 0.024713 * F_y + 8.29686 * f'_c - 0.034441 * t * h - 0.032151 * t * H - 6.91831E-3 * t * F_y + 0.010906 * t * f'_c - 1.77546E-4 * h * H - 1.43867E-3 * h * F_y + 1.15999E-3 * h * f'_c + 1.35156E-3 * H * F_y - 0.011532 * H * f'_c - 5.84854E-3 * F_y * f'_c - 0.036207 * t^2 - 7.41982E-5 * h^2 + 1.08895E-3 * H^2 + 1.02511E-3 * F_y^2 + 9.96057E-3 * {f'_c}^2 \quad (7)$$

$$S(t,h,H,F_y,f'_c) = +3276.60115 - 84.59325 * t - 8.51317 * h - 5.27956 * H - 4.27821 * F_y - 37.12463 * f'_c + 0.13301 * t * h + 0.079162 * t * H + 0.053758 * t * F_y + 0.50698 * t * f'_c + 7.65284E-3 * h * H + 6.77784E-3 * h * F_y + 0.040477 * h * f'_c + 5.24357E-3 * H * F_y + 0.032885 * H * f'_c +$$

$$0.029425 * F_y * f_c' + 0.47265 * t^2 + 4.26323E - 3 * h^2 + 6.92056E - 4 * H^2 + 7.30877E - 4 * F_y^2 + 0.10650 * f_c'^2 \quad (8)$$

Explicit mathematical formulas that show the relationship between load-bearing capacity and stress with the five problem variables are presented in Equations (7) and (8). Figure 13 shows the lower bearing capacity and stress derived from the finite elements extracted from the Abaqus software against the values obtained from the above equations expressed by the response surface. These plots show a very high coefficient of determination (R^2), indicating the prediction and interpolation accuracy of the presented formula.

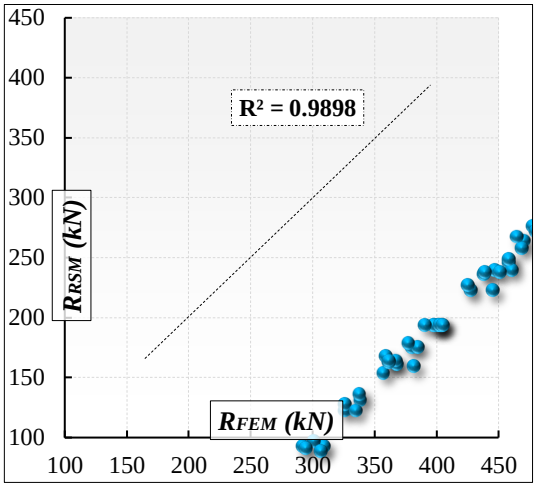

(a)

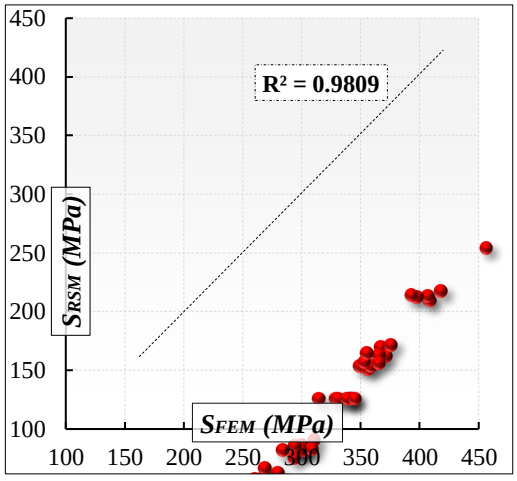

(b)

Fig. 13: (a) Correlation between finite element solution and response surface for load-bearing capacity, (b) correlation between finite element solution and response surface for stress

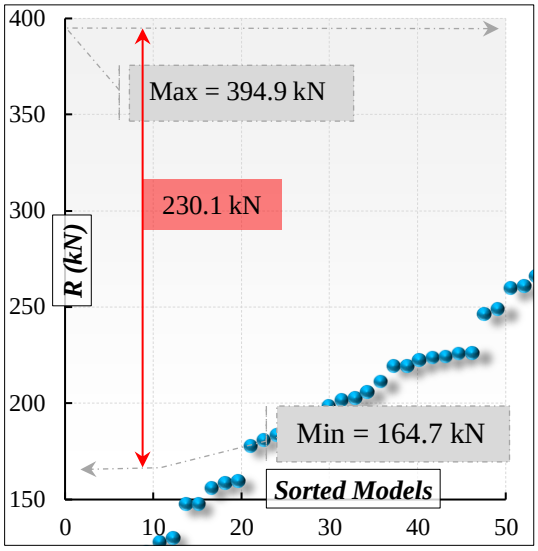

(a)

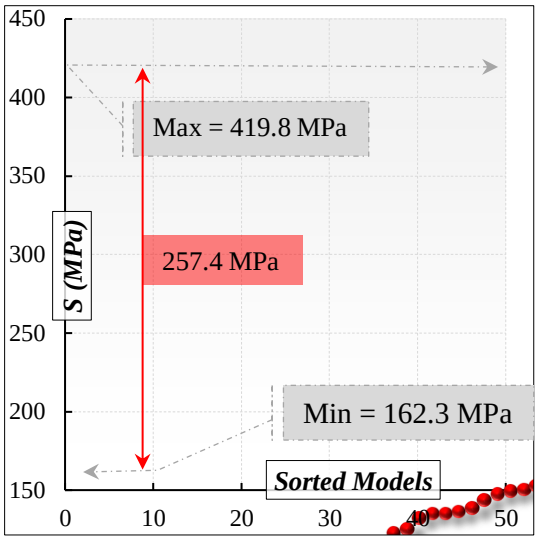

(b)

Fig. 14: (a) Sorting models based on load-bearing capacity, (b) sorting models based on stress

It is well known that increasing the load-bearing capacity of the model increases the maximum stress. Therefore, it is desirable to optimize the present functions so that a certain value does not exceed the load-bearing capacity by the model's maximum stress. This certain value is usually obtained when optimizing structures at the 85% level of the stress interval. In these conditions, the failure level in most incremental dynamics analyses (IDAs) is equal to 85% of the structure's response interval. Another parameter called gamma (Γ), which specifies the problem, is introduced by Equation (9):

$$\Gamma_\theta = [\xi * (Max_\theta - Min_\theta)] + Min_\theta \quad (9)$$

where Γ_θ is the maximum limit of parameter θ. In this study, θ denotes the stress of the system (S). Also, ξ shows the failure level, namely 85% (0.85) of the stress interval according to the explanations provided. The maximum (Max_θ) and minimum (Min_θ) values of the parameter in question should be subtracted to calculate this interval. In this way, the amount of stress at the resolution limit should be calculated:

$$\Gamma_S = [0.85 * (419.8 - 162.3)] + 162.3 = 381.175 \quad (10)$$

Therefore, Equation (11) states that structural failure occurs whenever the system stress is greater than 381.175 MPa, which is set as the problem boundary. As mentioned earlier, the problem has the objective function of maximizing the load-bearing capacity in Equation (8), as the Γ_S value in Equation (9) is defined (less than 381.175 MPa). Therefore, Equation (12) is defined as the current optimization problem:

$$maximize: \quad f(x) = R(t, h, H, F_y, f_c') \quad (11)$$
$$Subject\ to: \quad S(t, h, H, F_y, f_c') < \Gamma_S$$
$$In\ which:$$
$$\Gamma_S = 381.175\ (MPa)$$
$$6 \le t(mm) \le 14$$
$$60 \le h(mm) \le 140$$
$$120 \le H(mm) \le 280$$
$$260 \le F_y(MPa) \le 420$$
$$20 \le f_c'(MPa) \le 40$$

By substituting Equations (7) and (8) into the objective function related to the problem statement (11), we have:

$$\boldsymbol{maximize}: \quad R(t, h, H, F_y, f_c') = -444.22183 + 23.43675 * t + 2.02854 * h + 0.35536 * H + 0.024713 * F_y + 8.29686 * f_c' - 0.034441 * t * h - 0.032151 * t * H - 6.91831E-3 * t * F_y + 0.010906 * t * f_c' - 1.77546E-4 * h * H - 1.43867E-3 * h * F_y + 1.15999E-3 * h * f_c' + 1.35156E-3 * H * F_y - 0.011532 * H * f_c' - 5.84854E-3 * F_y * f_c' - 0.036207 * t^2 - 7.41982E-5 * h^2 + 1.08895E-3 * H^2 + 1.02511E-3 * F_y^2 + 9.96057E-3 * f_c'^2$$

$$\boldsymbol{Subject\ to}: \quad S(t, h, H, F_y, f_c') - \Gamma_S < 0 \rightarrow +3276.60115 - 84.59325 * t - 8.51317 * h - 5.27956 * H - 4.27821 * F_y - 37.12463 * f_c' + 0.13301 * t * h + 0.079162 * t * H + 0.053758 * t * F_y + 0.50698 * t * f_c' + 7.65284E-3 * h * H + 6.77784E-3 * h * F_y + 0.040477 * h * f_c' + 5.24357E-3 * H * F_y + 0.032885 * H * f_c' + 0.029425 * F_y * f_c' + 0.47265 * t^2 + 4.26323E-3 * h^2 + 6.92056E-4 * H^2 + 7.30877E-4 * F_y^2 + 0.10650 * f_c'^2 - 381.175 < 0 \quad (12)$$

Equation (13) is used to apply the penalty function to convert this bound problem into an unbound problem:

$$f_p(x) = f(x) + \lambda \sum_{k=1}^{m} \delta_k [g_k(x)]^2 \quad (13)$$

where λ should be more than 1 (in this study, $\lambda = 10^{15}$). It is noteworthy that this method can be improved by imposing a relative penalty. Thus, the effect on the changes in the objective function and the constraint is first evaluated as each variable changes, followed by the calibration of the values and the multiplication of λ for each variable. Also, parameter δ_k is defined by Equation (14) to show the violation event.

$$\begin{cases} \delta_k = 1\ if\ constraint\ g_k\ is\ violated \\ \delta_k = 0\ if\ constraint\ g_k\ is\ satisfied \end{cases} \quad (14)$$

The sensitivity analysis was performed to examine the effect of each variable on the response. The effect of the variation of each variable on the load-bearing capacity and stress is estimated in this analysis. In this way, the sensitivity of each parameter can be defined by Equation (15):

$$Sensitivity\ Analysis: \frac{\partial f(x)}{\partial x} = \frac{f(x+\Delta x)}{x+\Delta x} \rightarrow$$
$$in\ which: \begin{cases} f(x) \equiv [R, S] \\ x \equiv [t, h, H, F_y, f_c'] \end{cases} \quad (15)$$

where Δ represents the change rate of each variable. In certain sensitivity analyses, the rate of this change affects the response. However, it was found by trial and error in the current relation that a reduction of less than 1% in the interval of each variable does not make much difference in the response. Consequently, the changes were made in the form of $[x + 0.01(Max_x - Min_x)]$ for each variable. Therefore, the results are obtained by calculating the unit vector $\frac{\frac{f(x+\Delta x)}{x+\Delta x}}{\left|\frac{f(x+\Delta x)}{x+\Delta x}\right|}$. Table 4 shows the results of the sensitivity analysis. It should be noted that the values in Table 4 are in the form of a unit vector and equal to 1 in size.

Table. 3: Sensitivity analysis of relationships between load-bearing capacity and stress for five parameters of present problem

		$\frac{\partial f(x)}{\partial t}$	$\frac{\partial f(x)}{\partial h}$	$\frac{\partial f(x)}{\partial H}$	$\frac{\partial f(x)}{\partial F_y}$	$\frac{\partial f(x)}{\partial f_c'}$
$f(x) \rightarrow R$	Rate	0.3384	0.3692	0.3552	0.6461	0.4534
	Rank	5	3	4	1	2
$f(x) \rightarrow S$	Rate	-0.3619	-0.3705	-0.3918	-0.6234	-0.4356
	Rank	5	4	3	1	2

For each of the five problem variables, the results show an increase in the load-bearing capacity of the system and a reduction in the connection stress. Table 3 also describes the significance of the variables as rank for the change in the load-bearing capacity and stress. To view the results of the sensitivity analysis better, Figure 15 shows the rate of change in load-bearing capacity and stress for each variable.

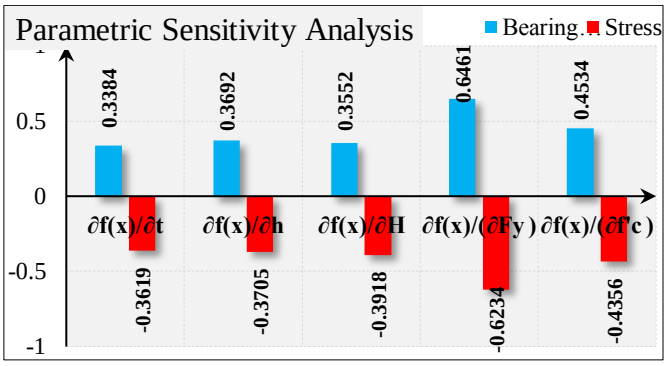

Fig. 15: Change rate of load-bearing capacity and stress against change of each variable

Thus, the constraints are applied to the problem and the optimization becomes an unbound problem (Equation 13). The optimization is performed in the following four different modes:

In the first case, 5 average particles (nA = 5) and 5 search particles (nS = 5) are used.

In the second case, 5 average particles (nA = 5) and 10 search particles (nS = 10) are used.

In the third case, 10 average particles (nA = 10) and 5 search particles (nS = 5) are used.
In the fourth case, 10 average particles (nA = 10) and 10 search particles (nS = 10) are used.
In each of the above cases, one hundred iterations of the algorithm are considered. The convergence schemes are shown in Figure 16 for each of the four modes. As mentioned above, the objective of the optimization is to maximize stress load capacity. Therefore, the best design is achieved by the fourth mode with 10,000 iterations, in which the load-bearing capacity of 3300.2901 kN and the stress of 381.067 MPa are obtained (10 median particles and 10 search particles per 100 iterations). The geometric parameters *t*, *h*, and *H* are, respectively, 12.83 mm, 135.49 mm, and 273.42 mm. The steel yield stress (F_y) and concrete strength (f_c') were found to be 416.38 MPa and 30.37 MPa, respectively.

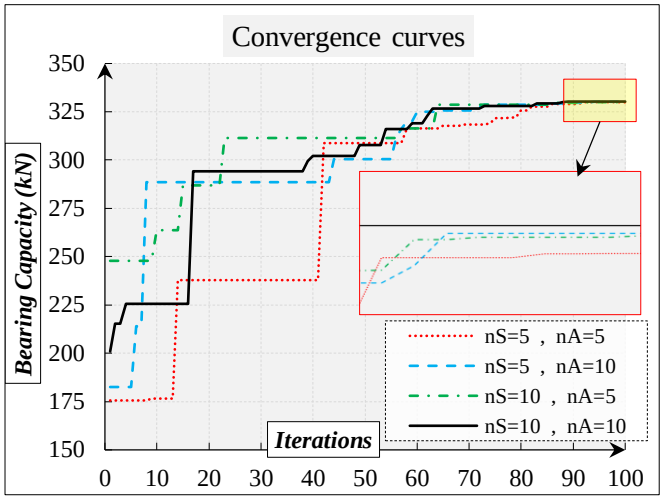

Fig. 16: Convergence diagrams for optimizing rib plate parameters

Again, the stress contour was derived (Figure. 17) after modeling the optimal design using the Abaqus software. The maximum stress in this model is 380.7 MPa, which differs only by 0.01% from the computer model developed by RSM.

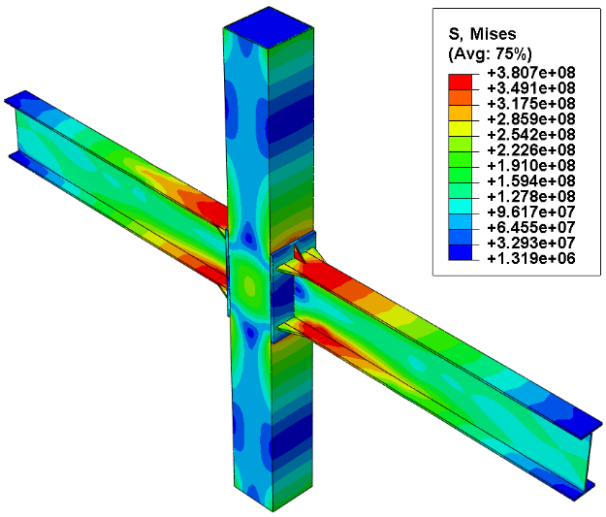

Fig. 17: Stress contours of optimal model

When estimating the load-bearing capacity of this model, the solution of ABAQUS was equal to 328.65 kN. In the optimization, this value differed from the calculated design by only 0.4%, which shows the accuracy of the calculations. The above model also shows the proper distribution of stresses and the use of an appropriate connection. In addition to the geometric parameters, the effects on the performance of the steel strength system and concrete consumption are very important. The influence of optimization is pronounced in the designed connection.

5. Conclusion

The present study deals with the geometric optimization and strength parameters for the connection of through-bolt steel beams to CFST columns reinforced with rib plates. The study by Wu LY et al. was considered as a reference and the Abaqus software was then used to calibrate and validate the FEM results. Subsequently, the problems were treated as variables with three geometric parameters and two material strength parameters. RSM was used to develop the necessary models to produce the objective function and problem constraint functions in this study. The optimization problem aimed to maximize the model's load-bearing capacity when the maximum system stress limit is of concern.
The multi-level cross-entropy optimizer (MCEO) algorithm was also considered as a solver, whose results have recently been shown to be more accurate than robust current algorithms. Finally, Abaqus software was used to design the optimal connection model. It correspondingly estimated the load-bearing capacity and stress and the optimal design of the designed model. The results obtained using RSM in developing the corresponding functions confirmed the correctness of the relationship. The correlation coefficient between load-bearing and stress was 0.9898 and 0.9809, respectively, which is very high and reasonable. This solution eliminates the need to link the finite element software with the MATLAB code and substantially reduces the computational cost. This solution can optimize the performance of several systems that require a large amount of analysis time and solve a wide range of structural problems. The results of the MCEO optimization algorithm were accurate with few search particles (25 particles per 100 iterations). With an average of 10 particles and 10 search particles in 100 iterations, the stress constraint was almost within the defined limit and thus the best result was obtained. The results obtained from the finite elements and RSM relationships were very consistent. It was also observed that the strength parameters have a greater influence on the connection response in the parametric sensitivity analysis of the connection. Failure to consider other geometric parameters, such as the dimensions of beams and columns, can be considered as one of the limitations of the current study.

References:

[1] Parvini Sani H, Gholhaki M, Banazadeh M. (2018). Simplified direct loss measure for seismic isolated steel moment-resisting structures. J Constr Steel Res, 147:313–23. https://doi.org/10.1016/j.jcsr.2018.04.010.

[2] Sani HP, Gholhaki M, Banazadeh M. (2017). Seismic Performance Assessment of Isolated Low-Rise Steel Structures Based on Loss Estimation. J Perform Constr Facil, 31:04017028. https://doi.org/10.1061/(ASCE)CF.1943-5509.0001028.
[3] Banazadeh M, Gholhaki M, Parvini Sani H. (2017). Cost-benefit analysis of seismic-isolated structures with viscous damper based on loss estimation. Struct Infrastruct Eng, 13:1045–55. https://doi.org/10.1080/15732479.2016.1236131.
[4] Kaveh A, Khodadadi N, Azar BF, Talatahari S. (2020). Optimal design of large-scale frames with an advanced charged system search algorithm using box-shaped sections. Eng Comput, https://doi.org/10.1007/s00366-020-00955-7.
[5] Alhaddad W, Halabi Y, Meree H, Yu Z. (2020). Optimum design method for simplified model of outrigger and ladder systems in tall buildings using genetic algorithm. Structures , 28:2467–87. https://doi.org/10.1016/j.istruc.2020.09.066.
[6] Das R, Steensels R, Dragan D, Vandoren B, Degée H. (2020). Characterization and optimization of a steel beam to RC wall connection for use in innovative hybrid coupled wall systems. Structures, 23:111–25. https://doi.org/10.1016/j.istruc.2019.10.011.
[7] Shehab M, Alshawabkah H, Abualigah L, AL-Madi N. (2020). Enhanced a hybrid moth-flame optimization algorithm using new selection schemes. Eng Comput, https://doi.org/10.1007/s00366-020-00971-7.
[8] Zou D, Gao L, Li S, Wu J. (2011). An effective global harmony search algorithm for reliability problems. Expert Syst Appl, 38(4):4642–48. https://doi.org/10.1016/j.eswa.2010.09.120.
[9] Mirjalili S. (2015). Moth-flame optimization algorithm: A novel nature-inspired heuristic paradigm. Knowledge-Based Syst, 89:228–49. https://doi.org/10.1016/j.knosys.2015.07.006.
[10] Zhang T. (2018). Robust reliability-based optimization with a moment method for hydraulic pump sealing design. Struct Multidiscip Optim, 58:1737–50. https://doi.org/10.1007/s00158-018-1996-1.
[11] Ami M, Zahrai SM. (2021). Effect of bolted shear connectors on the axial load-bending moment interaction capacity of CFT columns. Structures, 29:92–106. https://doi.org/10.1016/j.istruc.2020.10.072.
[12] Hassan MM, Ramadan HM, Abdel-Mooty M, Mourad SA. (2020). Seismic behavior of braced frames with different connection details to concrete filled tube columns. Structures, 28:2379–91. https://doi.org/10.1016/j.istruc.2020.10.031.
[13] Rezaifar O, Younesi A. (2017). Experimental study discussion of the seismic behavior on new types of internal/external stiffeners in rigid beam-to-CFST/HSS column connections. Constr Build Mater , 136:574–89. https://doi.org/10.1016/j.conbuildmat.2017.01.032.
[14] Han LH, Li W, Bjorhovde R. (2014). Developments and advanced applications of concrete-filled steel tubular (CFST) structures: Members. J Constr Steel Res, 100:211–28. https://doi.org/10.1016/j.jcsr.2014.04.016.
[15] Liang QQ. (2009). Performance-based analysis of concrete-filled steel tubular beam-columns, Part II: Verification and applications. J Constr Steel Res, 65(2):351–62. https://doi.org/10.1016/ j.jcsr.2008.03.003.
[16] Zhou G, An Y, Wu Z, Li D, Ou J. (2018). Analytical Model for Initial Rotational Stiffness of Steel Beam to Concrete-Filled Steel Tube Column Connections with Bidirectional Bolts. J Struct Eng, 144(11):04018199. https://doi.org/10.1061/(asce)st.1943-541x.0002187.
[17] Wu LY, Chung LL, Tsai SF, Lu CF, Huang GL. (2007). Seismic behavior of bidirectional bolted connections for CFT columns and H-beams. Eng Struct, 29(3):395–407. https://doi.org/10.1016/ j.engstruct.2006.05.007.
[18] Wang JF, Han LH, Uy B. (2009). Behaviour of flush end plate joints to concrete-filled steel tubular columns. J Constr Steel Res, 65(4):925–39. https://doi.org/10.1016/j.jcsr.2008.10.010.
[19] Wang J, Zhang N, Guo S. (2016). Experimental and numerical analysis of blind bolted moment joints to CFTST columns. Thin-Walled Struct, 109:185–201. https://doi.org/10.1016/j.tws.2016.07.017.
[20] Hanoon, A. N., Al Zand, A. W., & Yaseen, Z. M. (2021). Designing new hybrid artificial intelligence model for CFST beam flexural performance prediction. Engineering with Computers, 1–27.
[21] Nguyen, H. Q., Ly, H.-B., Tran, V. Q., Nguyen, T.-A., Le, T.-T., & Pham, B. T. (2020). Optimization of artificial intelligence system by evolutionary algorithm for prediction of axial capacity of rectangular concrete filled steel tubes under compression. Materials, 13(5), 1205.
[22] Yang, X., Yan, W., Chen, S., & Sun, H. (2010). Sequence optimization of concrete casting in steel tubular ribs for long-span CFST arch bridge. Journal of Highway and Transportation Research and Development, 27(1).
[23] Zhang, W., Chen, Z.-H., Xiong, Q.-Q., & Zhou, T. (2019). Seismic optimization analysis of vertical stiffener connection to L-CFST column. Advanced Steel Construction, 15(1), 100–108.
[24] G. Pachideh, M. Gholhaki, A. Moshtagh, Impact of Temperature Rise on the Seismic Performance of Concrete-Filled Double Skin Steel Columns with Prismatic Geometry, J. Test. Eval. 49 (2020).
[25] G. Pachideh, M. Gholhaki, A. Moshtagh, An Experimental Study on Cyclic Performance of the Geometrically Prismatic Concrete-Filled Double Skin Steel Tubular (CFDST) Columns, Iran. J. Sci. Technol. Trans. Civ. Eng. 45 (2021) 629–638.
[26] MiarNaeimi F, Azizyan G, Rashki M. (2018). Multi-level cross entropy optimizer (MCEO): an evolutionary optimization algorithm for engineering problems. Eng Comput, 34:719–739. https://doi.org/10.1007/s00366-017-0569-z.
[27] Tien CL, Lin SW. (2006). Optimization of process parameters of titanium dioxide films by response surfaces methodology. Opt Commun , 266(2):574–81. https://doi.org/10.1016/j.optcom.2006.05.044.
[28] Gayton N, Bourinet JM, Lemaire M. (2003). CQ2RS: A new statistical approach to the response surface method for reliability analysis. Struct Saf, 25(1):99–121. https://doi.org/10.1016/S0167-4730(02)00045-0.
[29] Zhang Z, Jiang C, Han X, Hu D, Yu S. (2014). A response surface approach for structural reliability analysis using evidence theory. Adv Eng Softw, 69:37–45. https://doi.org/10.1016/j.advengsoft.2013.12.005.
[30] Korumaz M, Betti M, Conti A, Tucci G, Bartoli G, Bonora V, et al. (2017). An integrated Terrestrial Laser Scanner (TLS), Deviation Analysis (DA) and Finite Element (FE) approach for health assessment of historical structures. A minaret case study. Eng Struct , 153:224–38. https://doi.org/10.1016/j.engstruct.2017.10.026.
[31] Wu LY, Chung LL, Tsai SF, Shen TJ, Huang GL. (2005). Seismic behavior of bolted beam-to-column connections for concrete filled steel tube. J Constr Steel Res, 61(10):1387–410. https://doi.org/10.1016/j.jcsr.2005.03.007.